Carbohydrate Polymers 90 (2012) 575–582

Contents lists available at SciVerse ScienceDirect

Carbohydrate Polymers

journal homepage: www.elsevier.com/locate/carbpol

Cellulose/polycaprolactone blends regenerated from ionic liquid 1-butyl-3-methylimidazolium chloride

Renyan Xiong, Nishar Hameed, Qipeng Guo*

Polymers Research Group, Institute for Frontier Materials, Deakin University, Geelong, Victoria 3216, Australia

ARTICLE INFO

Article history:
Received 23 September 2011
Received in revised form 20 May 2012
Accepted 22 May 2012
Available online 31 May 2012

Keywords:
Cellulose
Polycaprolactone
Blends
Ionic liquid

ABSTRACT

Ionic liquid solvent, 1-butyl-3-methylimidazolium chloride (BMIM[Cl]) was used to prepare cellulose/polycaprolactone (PCL) blend films. This solvent was recycled with high yield and purity after blend precipitation. The inter- and intra-molecular hydrogen bonding interactions in these blends were investigated by Fourier transform infrared (FTIR) spectroscopy and it was found that a new peak in the carbonyl region, assigned to hydrogen bonding between carbonyl groups of PCL and hydroxyl groups of cellulose in blends with PCL composition less than 40 wt%. Differential scanning calorimetry (DSC) results implied a partial miscibility of the two components by melting point depression. Moreover, the tensile properties of the blends can be adjusted by incorporating various amounts of PCL into cellulose. The blends show significant enhancement of thermal stability compared to the regenerated cellulose when the content of PCL is higher than 40 wt%. This work demonstrates an effective approach for the processing biodegradable blends from natural and synthetic polymers.

1. Introduction

Synthetic polymers have played an important role in modern society. However a serious threat to the environment has also arisen because of the non-biodegradable nature of plastics. Cellulose, as the most abundant renewable source in nature, is one of the attractive options as it is biodegradable and biocompatible. However the poor solubility of cellulose in water and many common solvents makes it difficult to process for many applications. Solvent systems for cellulose such as LiCl/*N*,*N*-dimethylacetamide (DMAc) (McCormick & Dawsey, 1990; Nishino, Matsuda, & Hirao, 2004; Nishio & Manley, 1998; Terbojevich, Cosani, Conio, Ciferri, & Bianchi, 1985; Williamson, Armentrout, Porter, & McCormick, 1998), LiCl/*N*-methyl-2-pyrrolidine (NMP) (Edgar, Arnold, Blount, Lawniczak, & Lowman, 1995), LiCl/1,3-dimethyl-2-imidazolidinone (DMI) (Tamai, Tatsumi, & Matsumoto, 2004), DMSO/paraformaldehyde (PF) (Masson & Manley, 1991a, 1991b), *N*-methylmorpholine-*N*-oxide (NMMO) (Heinze & Liebert, 2001), some molten salt hydrates (Fischer, Voigt, & Fischer, 1999; Hattori, Cuculo, & Hudson, 2002), and some aqueous solutions of metal complexes (Saalwächter & Burchard, 2001; Saalwächter et al., 2000) also confronted with various drawbacks such as volatility, toxicity and difficulty of recycle.

Swatloski, Spear, Holbrey, and Rogers (2002) and Zhang, Wu, Zhang, and He (2005) reported the use of ionic liquids as simple and non-derivatizing single component solvent for cellulose. Pulp cellulose can be dissolved in 1-butyl-3-methylimidazolium chloride (BMIM[Cl]) up to a concentration as high as 25 wt%. In addition, ionic liquids exhibit advantages such as non-volatility, easy recycling, non-flammability, thermal stability, etc., and based on these properties they have been referred to as green solvents. Although ionic liquids have contentious properties in terms of their green image considering their synthesis methods and disposal difficulties, there are currently many processes for the safe synthesis, recycle and reuse of ionic liquids (Blanchard & Brennecke, 2000; Renner, 2001).

Blending of polymers offers a simple and relatively cheap way to develop novel materials with a number of valuable properties. The miscibility and specific interaction of polymer blends have been of intensive interest due to strong economic incentives. In our previous work, the natural wool/cellulose-based blends (Hameed & Guo, 2009, 2010) and cellulose/poly (3-hydroxybutyrate-co-3-hydroxyvalerate) blends (Hameed, Guo, Tay, & Kazarian, 2011) were successfully prepared using BMIM[Cl]. In this study, we investigate the polymer blends of semi-crystalline PCL and microgranular cellulose processed in BMIM[Cl]. As one of the most common polyesters, polycaprolactone (PCL) is an industrially important polymer that is linear aliphatic, partially crystalline and biodegradable. Goldberg (1995) summarized the biodegradability of PCL and its utility in 1995 depicting the degradation mechanism of PCL with biodegradability study in a series of fungal growth,

* Corresponding author.
E-mail address: qguo@deakin.edu.au (Q. Guo).

0144-8617/$ – see front matter © 2012 Elsevier Ltd. All rights reserved.
http://dx.doi.org/10.1016/j.carbpol.2012.05.080

aerobic soil burial, compost and respirometry. Because of the biodegradability PCL is a promising alternation in the biodegradable materials field. Nishio and Manley (1990) investigated the miscibility and dynamic mechanical properties of cellulose/PCL blends prepared from DMAc-LiC1 solvent system. They concluded that an amorphous phase existed in cellulose/PCL blends where a limited amount of cellulose could be well mixed with PCL.

There are many advantages of blending modification of cellulose especially with a biodegradable polymer like PCL. Since both polymers are biodegradable, the blends films will presumably also be biodegradable behavior. The semi-crystalline nature of cellulose and PCL provide opportunity to study various phase behavior and crystalline morphology by varying the composition of the blend. There is a possibility of hydrogen bonding between the complimentary binding sites of cellulose and PCL and this will affect the blend morphology and other properties.

In our work, the miscibility, self-associated and inter-associated hydrogen bonds, crystallinity, thermal stability and mechanical properties of cellulose/PCL blends were investigated by DSC, FTIR, XRD, TGA, SEM and tensile testing techniques. The processing solvent BMIM[Cl] can be easily recycled via mixing with water, purified by distilling water away from the mixture. Our work provides an effective way to obtain entirely biodegradable blends from natural or synthetic polymer materials using ionic liquid as a solvent.

2. Experimental

2.1. Materials and preparation of regenerated cellulose/PCL blend films

Polycaprolactone (average $M_w \sim 14{,}000$, average $M_n \sim 10{,}000$ by GPC) was purchased from Aldrich. Microgranular cellulose was also a product from Aldrich. 1-Butyl-3-methylimidazolium chloride (BMIM[Cl]) was obtained from Fluka. The chemicals were all used as received.

The regenerated cellulose was prepared according to the literature (Hameed et al., 2011; Swatloski et al., 2002). A pre-weighed amount of cellulose was added to BMIM[Cl] in a 200 ml beaker, heated up to 90 °C and mechanically stirred for 1 h before PCL addition. The concentration of the solution was approximately 10 wt%. After PCL addition, the mixture was again stirred for another 24 h to allow complete mixing. Then the homogenous viscous solution was cast onto a plain glass plate, immersed in distilled water to remove BMIM[Cl] from the blends, since BMIM[Cl] is completely miscible with water at any ratio. After washing several times with deionized water, a white piece of regenerated cellulose/PCL blend film was obtained. The samples were first air dried then vacuum dried for 24 h before the tests. Photographs of cellulose/PCL blend films at different concentrations are shown in Fig. 1. The pure cellulose film is completely transparent with excellent flexibility. By increasing the PCL content, the films became translucent and will absolutely opaque at 20/80 cellulose/PCL blends. This may be due to the crystallization of the PCL component.

2.2. Characterization

2.2.1. Fourier transform infrared spectroscopy (FTIR)

FTIR spectra of cellulose/PCL blend films were recorded on a Bruker Vetex-70 FTIR spectrometer. For in situ spectra acquisition, the specimen was set in a variable temperature cell, which was then placed in the sample compartment equipped with a deuterated triglycine sulfate (DTGS) detector. The films were ground with KBr powder, pressed into round disk and vacuum dried overnight before the FTIR experiment. The transmission method at both room temperature and 80 °C was adopted. The spectra were recorded at average of 64 scans in the standard wave number range of 400–4000 cm^{-1} at a resolution of 4 cm^{-1}.

2.2.2. Differential scanning calorimetry (DSC)

A TA-DSC model Q200 instrument was used to determine melting temperature (T_m) and crystallization temperature (T_c) of the blends and crystallinity of the PCL component X_c (i.e. wt% of the crystallized PCL portion against the overall PCL component in the system). The sample weight for all testing was among 5–10 mg. All the samples were first heated to 100 °C at a rate of 20 °C/min, held for 5 min to remove the thermal history. The samples were then cooled to −80 °C at −20 °C/min, and subsequently heated again to 250 °C at 20 °C/min. T_m was taken as the endothermic peak position and T_c was evaluated from the exothermal peak position. And X_c was calculated from the peak area assuming that the heat of fusion for the perfect PCL crystal is 135 J/g. The equation for X_c calculation (Guo & Zheng, 1999; Zheng, Lu & Guo, 2004) was as following:

$$X_c = \frac{\Delta H_f}{\Delta H_f^0 \cdot X_n} \times 100\% \quad (1)$$

ΔH_f is the heat of fusion per gram; ΔH_f^0 is the perfect crystal heat of fusion of the crystallizable PCL; X_n is the weight percentage of PCL in blend materials.

2.2.3. Glancing-incidence asymmetric Bragg diffraction

X-ray diffraction patterns were obtained from Panalytical X'Pert PRO diffractometer with Cu Kα radiation (λ_1 = 1.5406 Å) at 40 kV and 30 mA. The recording range was 7–28° with a step size of 0.02° and a count time per step of 2 s on the parallel beam geometry. The samples are round shape films with 13 mm diameter. Glancing-incidence asymmetric diffraction was applied in order to increase the path length through the sample films and decrease the X-ray penetration into the holder. The weak reflections were enhanced via this measurement. Thickness correction has been applied for the scattering curves.

2.2.4. Thermogravimetric analysis (TGA)

Thermogravimetric analyses (TGA) were performed on Netzsch STA 409 thermogravimetric analyzer over a temperature range of 25–600 °C at a heating rate of 10 °C/min under nitrogen atmosphere. The nitrogen flow rate is 10 ml/min for the furnace purging and 30 ml/min to shield the balance. The onset decomposition temperature T_d is determined from the step tangent, which was taken as the onset of significant (≥0.5%) weight loss from the heated sample, after the moisture loss.

2.2.5. Scanning electron microscopy (SEM)

The morphology of the blends was examined with a Leica S440 scanning electron microscope (SEM) at an accelerating voltage of 20 kV. The cryo-fractured surfaces were coated with thin layers of gold before the observation via gold deposition technique under argon atmosphere. BAL-TEC SCD 050 sputter coater was used with a sputtering current of 40 mA and a sputtering time of 120 s.

2.2.6. Tensile test

The tensile properties of the blend films were analyzed using TA Q800 dynamic mechanical analyzer in tensile mode with ramp force to 18 N at a rate of 2 N/min. The specimen was a thin rectangular strip (20 mm × 4 mm). The load–displacement curves of the samples were obtained at room temperature. The stress and strain values were obtained using the standard equations as follows:

$$\text{Stress } \sigma = \frac{F}{A} \quad \text{strain } \varepsilon = \frac{\Delta L}{L}$$

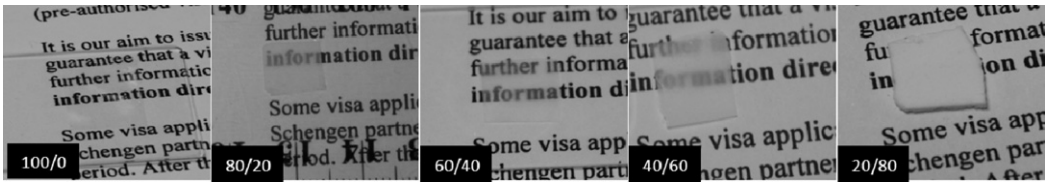

Fig. 1. Photographs of cellulose/PCL blend films (from left to right: 100/0; 80/20; 60/40; 40/60; 20/80).

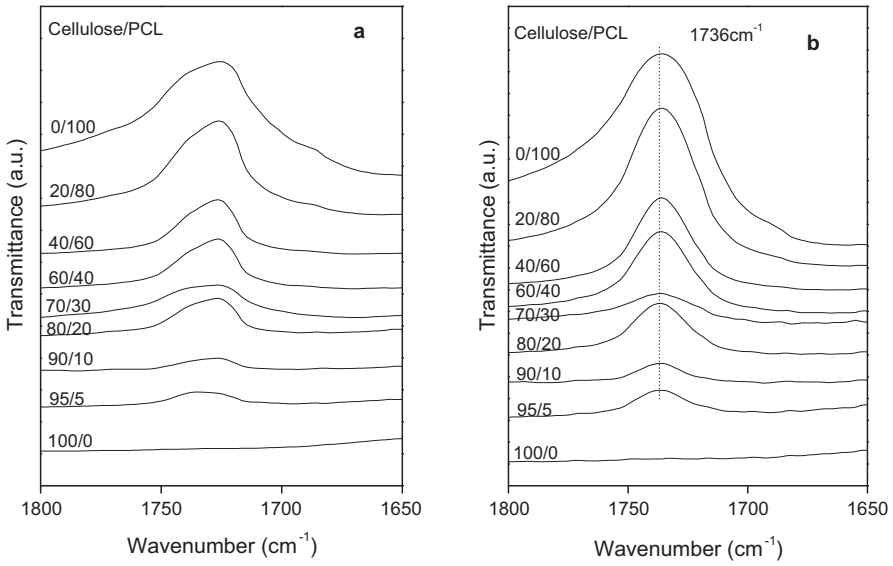

Fig. 2. Infrared spectra corresponding to the wavenumber region of 1650–1800 cm^{-1} of whole composition range cellulose/PCL blends at room temperature (a) and at 80 °C (b).

F is the loading force, A is the original specimen cross-sectional area, ΔL is the specimen displacement and L is the original specimen length.

The samples were kept under vacuum at 60 °C for one day before the tests and experiments were repeated with 5 samples of each composition.

3. Results and discussion

3.1. Hydrogen bonding interactions

It has been known that the specific interactions are driving force of the miscibility in polymer blends (Guo, 1990; Zheng, Guo & Mi, 1998). We employed FTIR spectroscopy to study the specific interactions in cellulose/PCL blend films. From Fig. 2, we can see that the shape of the room temperature FTIR spectra (Fig. 2a) changes with the increase in PCL content, while the shape of spectra obtained at temperature higher than the melting point of PCL was constant. The carbonyl region of the spectra shows a peak at 1736 cm^{-1}, corresponding to PCL amorphous state (Hameed & Guo, 2008; Hameed, Liu & Guo, 2008). For further information about the shape changing of the room temperature FTIR spectra, curve-fitting technique was adopted.

As for semicrystalline polymers, the IR spectra can generally be split into two peaks corresponding to the amorphous and crystalline phases. Here, PCL is a typical semicrystalline polymer (α,ω-hydroxyl functionalized polymer), which leads to a more complex phase situation. In Fig. 3a three carbonyl stretching regions were observed. The peaks at 1749 cm^{-1}, 1725 cm^{-1} and 1690 cm^{-1} were attributed to amorphous, crystalline and hydrogen bonded carbonyl stretching, respectively. Meanwhile, there is no peak for regenerated cellulose in this region. If there is no specific interactions between these two components, there will not be any peak shifting. Combining the experimental spectra with curve fitting, it is easy to notice the appearance of a new peak around 1685 cm^{-1}, corresponding to the hydrogen bonded carbonyl groups. From Table 1, the new peak 4 can reasonably be assigned to the carbonyl groups of PCL interacting with the hydroxyl groups of cellulose through hydrogen bonding. This indicates there is hydrogen bonding in the blends at compositions less than 40 wt% PCL. Moreover, the position for peak 1 shifted to higher frequency from 1690 cm^{-1} to 1705 cm^{-1}, indicating the hydrogen bonding strength between hydroxyl group and carbonyl group decreased. The frequency difference between the free carbonyl absorption and that of the hydrogen bonding species ($\Delta\nu$) is a measure of the average strength of the intermolecular interactions (Purcell & Drago, 1967). The position of peak 2 for the PCL crystallized carbonyl group was constant. While the peak for the amorphous PCL carbonyl bands shifted to lower frequency

Table 1
The fitted IR peaks in the carbonyl stretching region of cellulose/PCL blends via curve fitting technique.

Cellulose/PCL (wt%)	Peak 1 (cm^{-1})	Peak 2 (cm^{-1})	Peak 3 (cm^{-1})	Peak 4 (cm^{-1})
100/0	–	–	–	–
95/5	1705	1726	1737	1687
90/10	1706	1725	1737	1683
80/20	1700	1725	1738	1685
70/30	1700	1726	1738	1685
60/40	1699	1726	1737	–
40/60	1696	1727	1738	–
20/80	1692	1728	1740	–
0/100	1690	1725	1749	–

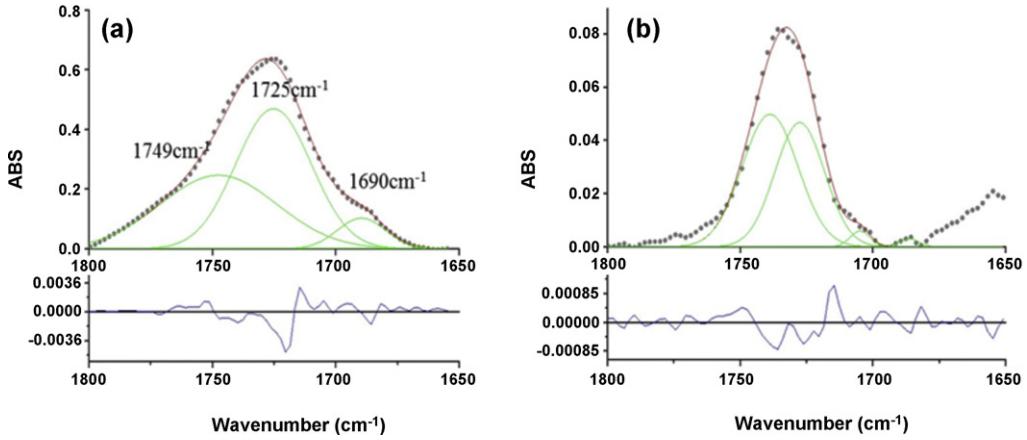

Fig. 3. Experimental and curve-fitted FTIR spectra of the PCL carbonyl stretching region in cellulose/PCL blend films. Cellulose/PCL: (a) 0/100; (b) 95/5; black line: experimental spectrum; red line: curve-resolved spectrum; green lines: fitted peaks. (For interpretation of the references to color in this figure legend, the reader is referred to the web version of the article.)

further confirmed the interaction between regenerated cellulose and PCL. As the regenerated cellulose content increases, the amount of amorphous PCL carbonyl groups increases deteriorating the intensity of crystallized carbonyl absorption, which hints that the regenerated cellulose lowers the PCL crystallinity. For clarity, we give a sketch of the hydrogen bonding interactions in regenerated cellulose/PCL blends in Fig. 4.

3.2. Phase behavior and crystallization

DSC was used to investigate the phase behavior and crystallization behavior of cellulose/PCL blends. In the first heating scan (Fig. 5), it is clear that the cellulose/PCL blends show melting point depression phenomenon, which is a characteristic feature of miscible polymer blends (Zheng, Zheng, & Guo, 1997a, 1997b; Zhong & Guo, 1998). For pure PCL, the pronounced melting temperature is at 66 °C, whereas the melting points of all blends are lower than this value indicating that a certain micibility between PCL and regenerated cellulose exists in the amorphous phase (Senda, He & Inoue, 2002). The broad melting peak for pure PCL at low temperature other than 66 °C is the melting of the less perfect PCL crystals, since its crystallinity is 62.7% as depicted in Fig. 8. In addition, a shoulder peak for 20/80 cellulose/PCL blend and a singular melting peak for 40/60 cellulose/PCL blend at around 54 °C are attributed to the less perfect crystallizd PCL portion melt and recrystallizing into higher order forms (Bogdanov, Vidts, Schacht, & Berghmans, 1999).

In the cooling scan, the crystallization behavior can be observed. In Fig. 6, the crystallization temperature for the blends increased with increasing cellulose composition, which suggested that the crystallization of PCL in the blends was affected by the addition of regenerated cellulose. Generally speaking, crystallization is a phase transition that is dominated by nucleation and the kinetics of growth (Wunderlich, 1976). The addition of regenerated cellulose has two different influences on PCL crystallization. On one hand, regenerated cellulose acts as a nucleating surface for PCL, which accelerates the crystallization of PCL. However, on the other hand, cellulose molecular chains also sterically restrict the PCL spherulitic growth, which hinders PCL crystallization. These

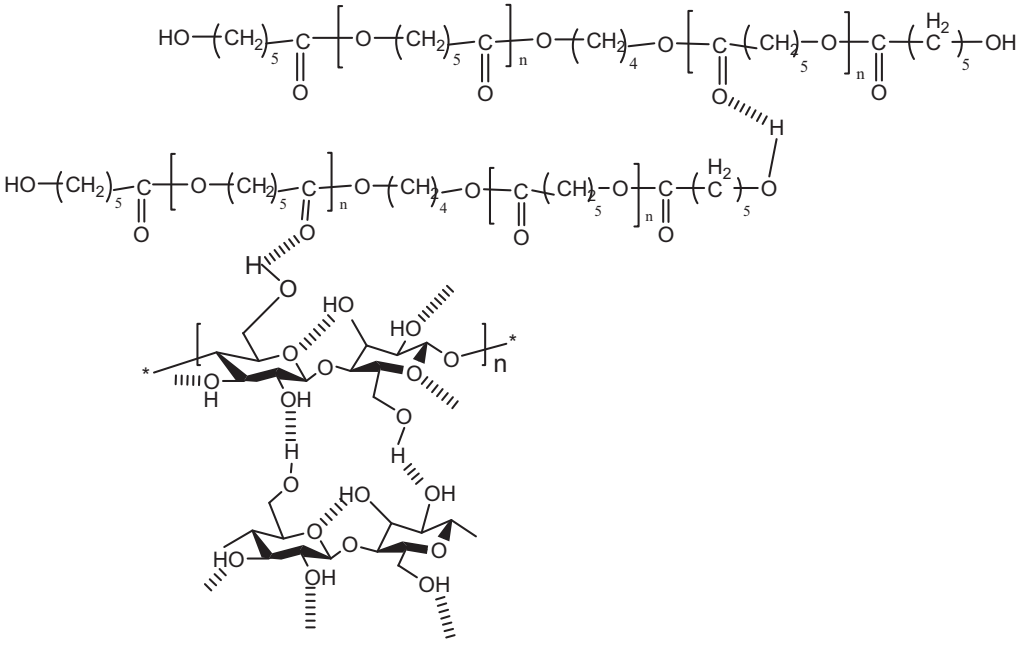

Fig. 4. Sketch of hydrogen bonding in cellulose/PCL blends.

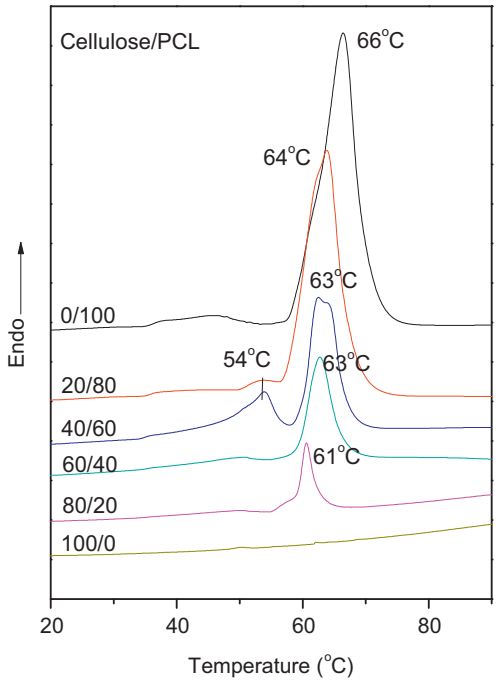

Fig. 5. Selected regions DSC curves of the first heating scan for cellulose/PCL blends.

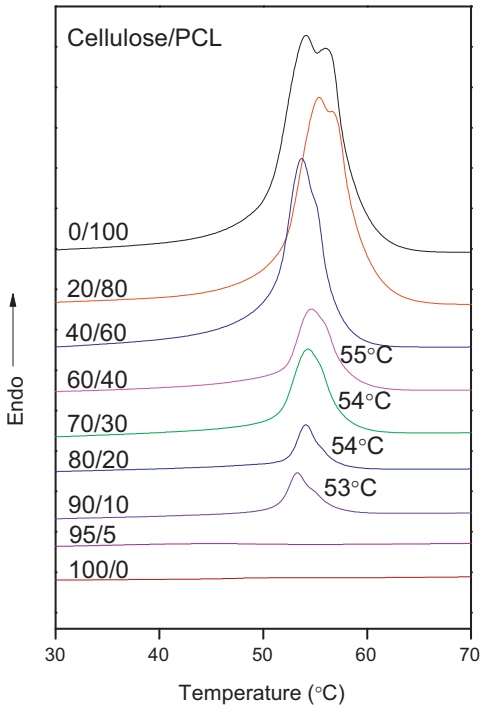

Fig. 7. Selected regions DSC curves of the second heating scan for cellulose/PCL blends.

two opposite effects compete and together determine the final effect of regenerated cellulose on PCL crystallization. Combining Fig. 8 and Fig. 10, the crystallinity and crystal size of PCL decreased sharply with the increasing of regenerated cellulose content. As shown in Fig. 8, pure PCL homopolymer is a partially crystallized polymer with a crystallinity of around 62.7%. Upon blending with cellulose, the crystallinity decreased sharply till 5.7% for 80/20 cellulose/PCL blend. In Fig. 10, the diameter of PCL spherulites decreased from approximately 110–160 μm to 10–25 μm with addition of 80 wt% cellulose. Furthermore, the crystallization temperature for the blends increased approximately 30% by addition of 80 wt% regenerated cellulose, indicating the crystallization rate increased (Gupta & Purwar, 1984). Therefore it can be assumed that regenerated cellulose can facilitate the crystallization of PCL in these blends.

In Fig. 7, the DSC curves for melt-recrystallized samples are shown. We can see that after the removal of thermal history the endothermic peak positions all shift to low temperature compared with those as-coagulated ones. However, there still has a slight tendency of melting temperature depression with the increasing of cellulose content for compositions ranging from 60/40 to

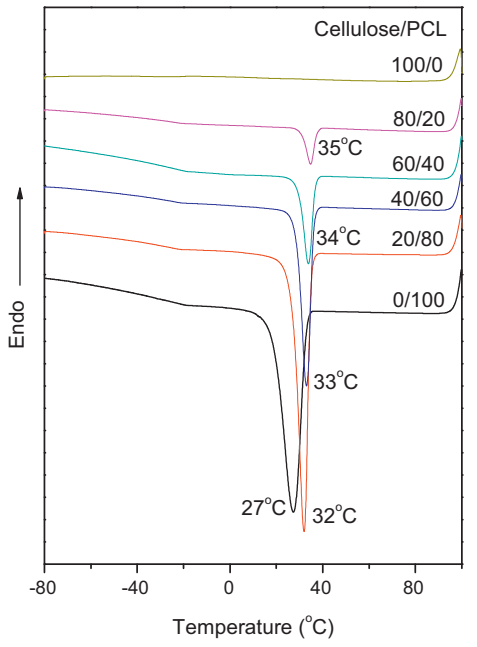

Fig. 6. Selected regions DSC curves of the cooling scan for cellulose/PCL blends.

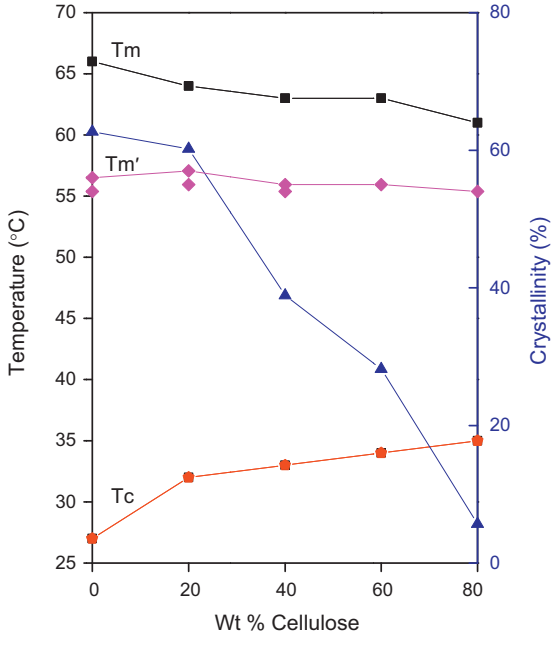

Fig. 8. Experimental T_m (■) of as-coagulated samples, T_m' (♦) of melt-recrystallized samples, T_c (⬟) and crystallinity (▲) versus blend compositions for cellulose/PCL blends.

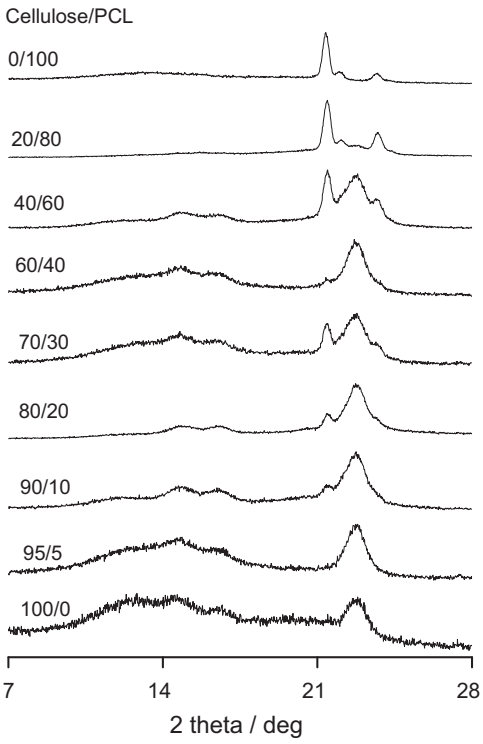

Fig. 9. Glancing-incidence diffraction analysis of cellulose/PCL blend films.

90/10 cellulose/PCL blends, suggesting partial miscibility of PCL with regenerated cellulose. The driving force for this miscibility is hydrogen bonding between carbonyl groups of PCL and hydroxyl groups of cellulose. This result is consistent with the FTIR data.

The thermodynamic data obtained by analysis of the DSC curves are displayed in Fig. 8. Here the composition dependence of the T_m and T_c together with the crystallinity of PCL is plotted against cellulose content in the blends. From the curves, we can readily see that the PCL X_c value decreases with an increase of cellulose and slight melting point depression phenomenon exists. The T_c value increases reversely to the tendency of T_m, indicating the crystallization of PCL molecular is facilitated by the cellulose component in the cellulose/PCL blends.

Glancing-incidence diffraction analyses were used to follow the evolution of structure for PCL and cellulose and the results are given in Fig. 9. Pure PCL diffractograms show three characteristic reflections at 21.5°, 22.0° and 23.7° associated with the (1 1 0), (1 1 1) and (2 0 0) planes of the orthorhombic PCL lattice (Chen & Wu, 2007). For regenerated cellulose, the characteristic peaks are 12.4°, 14.77°, 16.65° and 22.77°, which are the combination of both cellulose I and cellulose II reflection peaks (Takahashi & Matsunaga, 1991; Zhang et al., 2005). However, the former three peaks are less well defined, which is attributed to the increase in the amount of amorphous cellulose after regeneration from the BMIM[Cl] solution. In cellulose rich blends (PCL content less than 40 wt%), the characteristic diffraction peak 23.7° for PCL crystal is not pronounced. For PCL rich blends (PCL content more than 40 wt%), the XRD patterns are mainly attributed to the PCL phase. The peaks for regenerated cellulose at these compositions can be neglected because of the weak intensity. For 60/40 cellulose/PCL blend, the intensity of the two reflection peaks for PCL (2θ = 21.5° and 23.7°) are substantially reduced. It is suggested that not only the cellulose chain sterically inhibits the crystallization of PCL, but also the hydrogen bonding interaction between cellulose and PCL restrains the movement of PCL molecules and even partially destroys the original crystalline structure of PCL, and consequently decreases PCL crystallinity upon blending. The curve for 40/60 cellulose/PCL blend is just a summation of the PCL and regenerated cellulose crystal patterns, indicating that PCL and cellulose can form individual crystal phases; that are two separate microdomains in this composition. This result will be further discussed in Section 3.3.

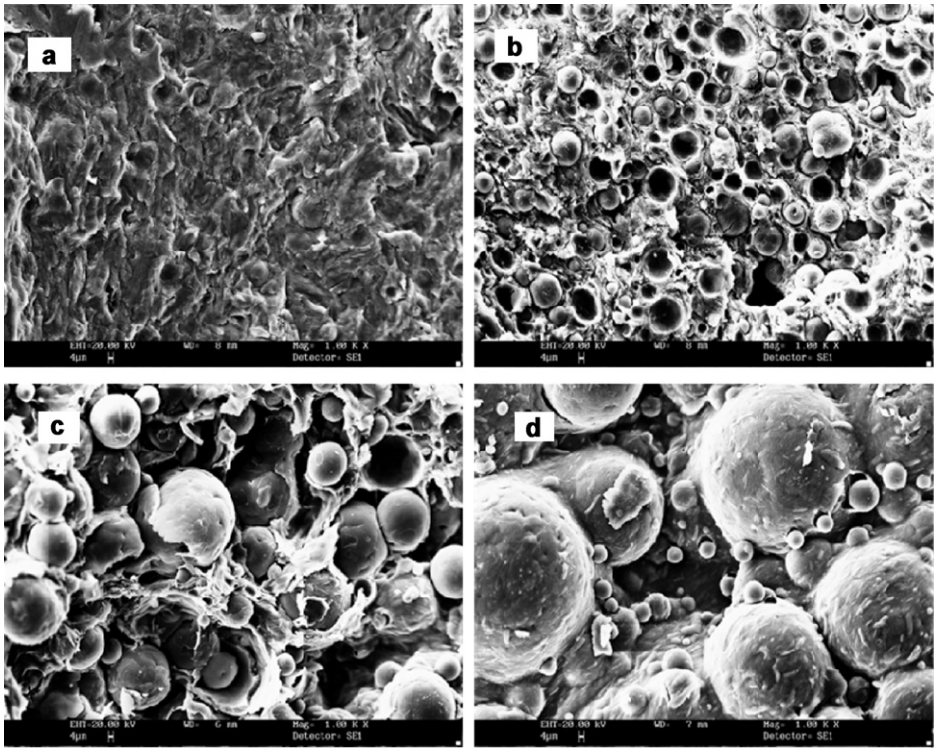

Fig. 10. Scanning electron micrographs of the cryo-fractured surfaces of (a) 80/20, (b) 60/40, (c) 40/60, and (d) 20/80 cellulose/PCL blends.

Table 2
The tensile properties of cellulose/PCL blends.

Cellulose/PCL (wt%)	Young's modulus (GPa)	Tensile strength (MPa)	Elongation at break (%)
100/0	3.58 ± 0.04	74.5 ± 1.6	4.0 ± 0.30
80/20	1.39 ± 0.34	21.4 ± 4.1	2.2 ± 0.45
60/40	2.48 ± 0.65	15.2 ± 2.5	1.1 ± 0.28
40/60	1.32 ± 0.24	4.7 ± 0.7	0.4 ± 0.06

3.3. Morphology of regenerated cellulose/PCL blends

Scanning electron microscopy was employed to study the morphology of the blends. Further to the real images of the component distribution, liquid nitrogen was introduced to get cryo-fractured surfaces. Swatloski et al. (2002) reported that after regeneration of cellulose from BMIM[Cl], the morphology of the cellulose was significantly changed to a rough, but conglomerate texture in which the fibers are fused into a relatively homogeneous macrostructure. In general, the cellulose/PCL blends exhibit fine blend morphologies with dispersed PCL phase domains, which are spherical in shape. With the PCL content increasing, the dispersing domains expanded as well as the spherical diameter increases. For 80/20 cellulose/PCL blend (Fig. 10a), the SEM image shows random small PCL beads distributed in the rough conglomerate texture with diameter range of 10–25 μm. As to 60/40 cellulose/PCL blend, the PCL beads become evenly distributed in the continuously regenerated cellulose matrix, the size for the beads are roughly the same as 80/20 cellulose/PCL sample. PCL chains are confined to this small region by predominant amount of cellulose and are unable to form high ordered crystal structure, which result in less crystallinity and almost the complete absence of PCL crystal pattern in corresponding XRD curve. By increasing the PCL content to 60 wt% of the total weight, the size of PCL beads increased to a range of 20–80 μm (Fig. 10c). Micro-phase separation is obvious and the regenerated cellulose domain is not as continuous as the 60/40 cellulose/PCL blend. The confinement of the cellulose chains for PCL crystallization is weakened hence both component crystal patterns are presented in XRD curve. Further increase the PCL content to 80 wt% of the total weight, the PCL spheres become the dominant phase, an interesting phenomena is that there are two main PCL sphere size, one is as large as 110–160 μm, while the other is as small as 6–20 μm (Fig. 10d). It is obvious that the surface of the bigger sphere is rough with a worm-like texture on while the smaller ones have a rather smooth surface. The reason for this may be the regenerated cellulose coated on some of the PCL spheres to form the bigger ones with the excess of PCL amount and some other PCL particles are left alone. A limited amount of cellulose can be well mixed with PCL especially at the compositions containing 20 and 30 wt% cellulose. The melting behaviors for these two size beads are different. Combining the DSC data in Fig. 5, the shoulder peak at 54 °C can be assigned to the less developed crystal region and the corresponding content is relatively low resulting in the low intensity of this exothermic shoulder peak.

3.4. Mechanical properties and thermal stability

Mechanical properties of polymer blends are generally dependent to their miscibility and phase structure (Guo et al., 1990; Zheng, Hu, Guo, & Wei, 1996; Zhong et al., 1998). The mechanical properties of the cellulose/PCL blends were also investigated. Young's modulus, tensile strength and elongation at break are all summarized in Table 2. It is obviously seen that regenerated cellulose exhibit the highest tensile strength as well as Young's modulus. As the PCL content increased, the tensile strength and elongation at break decrease dramatically. This may due to the incorporation of less strong PCL component into regenerated cellulose. For PCL rich blend films, the tensile properties are not able to be studied because their highly brittle behavior.

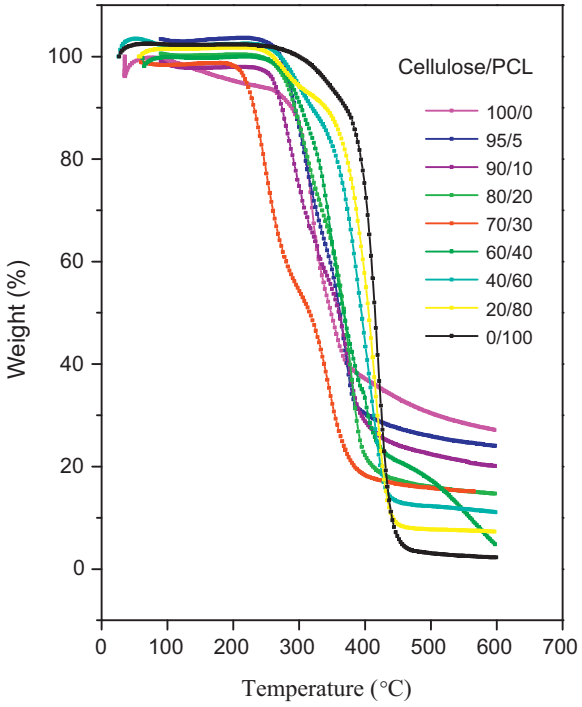

Fig. 11. TGA curves for cellulose/PCL blends. (For interpretation of the references to color in this artwork, the reader is referred to the web version of the article.)

The thermal stability of the cellulose/PCL blends was examined by thermogravimetric analyses. The results are shown in Fig. 11 and it shows there are two active weight loss steps. The first step about 250–300 °C due to the disassociation of intermolecular side chains; the second step round 300–600 °C corresponding to the chemical reactions between the main chains (Prasad et al., 2011). The T_{onset} for regenerated cellulose is only 270 °C. The onset decomposition temperature for the blends first increases then decreases with the increasing of the PCL content. At 60 wt% of PCL concentration, the material enhanced its thermal stability to 404 °C, which is around 30% improvement compared to the neat cellulose. Combining with the former data, it is further revealed that there is intra-molecular interaction between regenerated cellulose and PCL which improves the thermal stability of the blends.

4. Conclusions

In this study, cellulose/PCL blend films were successfully prepared using ionic liquid solvent BMIM[Cl]. The regenerated blends show partial miscibility between cellulose and PCL in the regenerated blends. The new peak region observed in FTIR curves of the blends with less than 40 wt% of PCL composition revealed the existence of hydrogen bonds between carbonyl group of PCL and hydroxyl group of cellulose. Crystallinity of the blends decreased dramatically with the increasing of cellulose composition. Moreover, the PCL phase exhibited spherical domains structure which was dispersed in continuous regenerated cellulose matrix in SEM observation. The beadlike microdomain size enlarged from 6–20 μm to 110–160 μm with the increasing PCL content. The tensile strength and elongation at break of the blends gradually decreased with increasing PCL concentration.

References

Blanchard, L. A., & Brennecke, J. F. (2000). Recovery of organic products from ionic liquids using supercritical carbon dioxide. *Industrial & Engineering Chemistry Research*, *40*, 287–292.

Bogdanov, B., Vidts, A., Schacht, E., & Berghmans, H. (1999). Isothermal crystallization of poly(ε-caprolactone ethylene glycol) block copolymers. *Macromolecules*, *32*, 726–731.

Chen, E.-C., & Wu, T.-M. (2007). Isothermal crystallization kinetics and thermal behavior of poly(ε-caprolactone)/multi-walled carbon nanotube composites. *Polymer Degradation and Stability*, *92*, 1009–1015.

Edgar, K., Arnold, K., Blount, W., Lawniczak, J., & Lowman, D. (1995). Synthesis and properties of cellulose acetoacetates. *Macromolecules*, *28*, 4122–4128.

Fischer, S., Voigt, W., & Fischer, K. (1999). The behaviour of cellulose in hydrated melts of the composition $LiX{\cdot}nH_2O$ ($X = I^-$, NO_3^-, CH_3COO^-, ClO_4^-). *Cellulose*, *6*, 213–219.

Goldberg, D. (1995). A review of the biodegradability and utility of poly(caprolactone). *Journal of Polymers and the Environment*, *3*, 61–67.

Guo, Q. (1990). Miscibility of poly(N-vinyl-2-pyrrolidone) with poly(vinyl chloride) and poly(epichlorohydrin). *Makromolekulare Chemie: Rapid Communications*, *11*, 279–283.

Guo, Q., Huang, J., Chen, T., Zhang, H., Yang, Y., Hou, C., et al. (1990). Mechanical properties of miscible phenolphthalein poly(ether ether ketone)/polysulfone blends. *Polymer Engineering and Science*, *30*, 44–48.

Guo, Q., & Zheng, H. (1999). Miscibility and crystallization of thermosetting polymer blends of unsaturated polyester resin and poly(ε-caprolactone). *Polymer*, *40*, 637–646.

Gupta, A. K., & Purwar, S. N. (1984). Crystallization of PP in PP/SEBS blends and its correlation with tensile properties. *Journal of Applied Polymer Science*, *29*, 1595–1609.

Hameed, N., & Guo, Q. (2008). Selective hydrogen bonding and hierarchical nanostructures in poly(hydroxyether of bisphenol A)/poly(ε-caprolactone)-block-poly(2-vinyl pyridine) blends. *Polymer*, *49*, 922–933.

Hameed, N., & Guo, Q. (2009). Natural wool/cellulose acetate blends regenerated from the ionic liquid 1-butyl-3-methylimidazolium chloride. *Carbohydrate Polymers*, *78*, 999–1004.

Hameed, N., & Guo, Q. (2010). Blend films of natural wool and cellulose prepared from an ionic liquid. *Cellulose*, *17*, 803–813.

Hameed, N., Guo, Q., Tay, F. H., & Kazarian, S. G. (2011). Blends of cellulose and poly(3-hydroxybutyrate-co-3-hydroxyvalerate) prepared from the ionic liquid 1-butyl-3-methylimidazolium chloride. *Carbohydrate Polymers*, *86*, 94–104.

Hameed, N., Liu, J., & Guo, Q. (2008). Self-assembled complexes of poly(4-vinylphenol) and poly(ε-caprolactone)-block-poly(2-vinylpyridine) via competitive hydrogen bonding. *Macromolecules*, *41*, 7596–7605.

Hattori, K., Cuculo, J. A., & Hudson, S. M. (2002). New solvents for cellulose: Hydrazine/thiocyanate salt system. *Journal of Polymer Science Part A: Polymer Chemistry*, *40*, 601–611.

Heinze, T., & Liebert, T. (2001). Unconventional methods in cellulose functionalization. *Progress in Polymer Science*, *26*, 1689–1762.

Masson, J. F., & Manley, R. S. J. (1991a). Cellulose/poly (4-vinylpyridine) blends. *Macromolecules*, *24*, 5914–5921.

Masson, J. F., & Manley, R. S. J. (1991b). Miscible blends of cellulose and poly(vinylpyrrolidone). *Macromolecules*, *24*, 6670–6679.

McCormick, C. L., & Dawsey, T. R. (1990). Preparation of cellulose derivatives via ring-opening reactions with cyclic reagents in lithium chloride/N,N-dimethylacetamide. *Macromolecules*, *23*, 3606–3610.

Nishino, T., Matsuda, I., & Hirao, K. (2004). All-cellulose composite. *Macromolecules*, *37*, 7683–7687.

Nishio, Y., & Manley, R. S. J. (1990). Blends of cellulose with nylon 6 and poly (ε-caprolactone) prepared by a solution coagulation method. *Polymer Engineering and Science*, *30*, 71–82.

Nishio, Y., & Manley, R. S. J. (1998). Cellulose-poly(vinyl alcohol) blends prepared from solutions in N,N-dimethylacetamide-lithium chloride. *Macromolecules*, *21*, 1270–1277.

Prasad, C. V., Sudhakar, H., Swamy, B. Y., Reddy, G. V., Reddy, C. L. N., Suryanarayana, C., et al. (2011). Miscibility studies of sodium carboxymethylcellulose/poly(vinyl alcohol) blend membranes for pervaporation dehydration of isopropyl alcohol. *Journal of Applied Polymer Science*, *120*, 2271–2281.

Purcell, K. F., & Drago, R. S. (1967). Theoretical aspects of the linear enthalpy wavenumber shift relation for hydrogen-bonded phenols. *Journal of the American Chemical Society*, *89*, 2874–2879.

Renner, R. (2001). Ionic liquids: An industrial cleanup solution. *Environmental Science & Technology*, *35*, 410A–413A.

Saalwächter, K., & Burchard, W. (2001). Cellulose in new metal-complexing solvents. 2. Semidilute behavior in Cd-tren. *Macromolecules*, *34*, 5587–5598.

Saalwächter, K., Burchard, W., Klüfers, P., Kettenbach, G., Mayer, P., Klemm, D., et al. (2000). Cellulose solutions in water containing metal complexes. *Macromolecules*, *33*, 4094–4107.

Senda, T., He, Y., & Inoue, Y. (2002). Biodegradable blends of poly (ε-caprolactone) with chitin and chitosan: Specific interactions, thermal properties and crystallization behavior. *Polymer International*, *51*, 33–39.

Swatloski, R. P., Spear, S. K., Holbrey, J. D., & Rogers, R. D. (2002). Dissolution of cellulose with ionic liquids. *Journal of the American Chemical Society*, *124*(18), 4974–4975.

Takahashi, Y., & Matsunaga, H. (1991). Crystal structure of native cellulose. *Macromolecules*, *24*, 3968–3969.

Tamai, N., Tatsumi, D., & Matsumoto, T. (2004). Rheological properties and molecular structure of tunicate cellulose in LiCl/1,3-dimethyl-2-imidazolidinone. *Biomacromolecules*, *5*, 422–432.

Terbojevich, M., Cosani, A., Conio, G., Ciferri, A., & Bianchi, E. (1985). Mesophase formation and chain rigidity in cellulose and derivatives. 3. Aggregation of cellulose in N,N-dimethylacetamide-lithium chloride. *Macromolecules*, *18*, 640–646.

Williamson, S. L., Armentrout, R. S., Porter, R. S., & McCormick, C. L. (1998). Microstructural examination of semi-interpenetrating networks of poly(N,N-dimethylacrylamide) with cellulose or chitin synthesized in lithium chloride/N,N-dimethylacetamide. *Macromolecules*, *31*, 8134–8141.

Wunderlich, B. (1976). *Macromolecular physics: Crystal nucleation, growth, annealing*. New York: Academic Press.

Zhang, H., Wu, J., Zhang, J., & He, J. (2005). 1-Allyl-3-methylimidazolium chloride room temperature ionic liquid: A new and powerful nonderivatizing solvent for cellulose. *Macromolecules*, *38*, 8272–8277.

Zheng, H., Zheng, S., & Guo, Q. (1997a). Thermosetting polymer blends of unsaturated polyester resin and poly(ethylene oxide). 1. Miscibility and thermal properties. *Journal of Polymer Science Part A: Polymer Chemistry*, *35*, 3161–3168.

Zheng, H., Zheng, S., & Guo, Q. (1997b). Thermosetting polymer blends of unsaturated polyester resin and poly(ethylene oxide). 2. Hydrogen-bonding interaction, crystallization kinetics, and morphology. *Journal of Polymer Science Part A: Polymer Chemistry*, *35*, 3169–3179.

Zheng, S., Guo, Q., & Mi, Y. (1998). Examination of miscibility at molecular level of poly(hydroxyether of bisphenol A) poly(N-vinyl pyrrolidone) blends by cross-polarization magic angle spinning C-13 nuclear magnetic resonance spectroscopy. *Journal of Polymer Science Part B: Polymer Physics*, *36*, 2291–2300.

Zheng, S., Hu, Y., Guo, Q., & Wei, J. (1996). Miscibility, morphology and fracture toughness of epoxy resin/poly(vinyl acetate) blends. *Colloid and Polymer Science*, *274*, 410–417.

Zheng, S., Lu, H., & Guo, Q. (2004). Thermosetting blends of polybenzoxazine and poly(ε-caprolactone): Phase behavior and intermolecular specific interactions. *Macromolecular Chemistry and Physics*, *205*, 1547–1558.

Zhong, Z., & Guo, Q. (1998). Miscibility and morphology of thermosetting polymer blends of novolac resin with poly(ethylene oxide). *Polymer*, *39*, 517–523.

Zhong, Z., Zheng, S., Huang, J., Cheng, X., Guo, Q., & Wei, J. (1998). Phase behaviour and mechanical properties of epoxy resin containing phenolphthalein poly(ether ether ketone). *Polymer*, 1075–1080.